

Experimental investigation of long-term characteristics of greenschist

Qing-Zhao Zhang^{1,2}, Ming-Rong Shen^{1,3}, Wen-Qi Ding^{1,3},
Hyun-Sic Jang² and Bo-An Jang^{*2}

¹ Department of Geotechnical Engineering, College of Civil Engineering,
Tongji University, Shanghai, SH 200092, China

² Department of Geophysics, Kangwon National University,

1 Kangwondaehak-gil, Chuncheon, Gangwon-do 24341, Republic of Korea

³ Key Laboratory of Geotechnical and Underground Engineering of Ministry of Education,
Tongji University, Shanghai, SH 200092, China

(Received September 14, 2015, Revised May 16, 2016, Accepted June 03, 2016)

Abstract. The greenschist in the Jinping II Hydropower Station in southwest China exhibits continuous creep behaviour because of the geological conditions in the region. This phenomenon illustrates the time-dependent deformation and progressive damage that occurs after excavation. In this study, the responses of greenschist to stress over time were determined in a series of laboratory tests on samples collected from the access tunnel walls at the construction site. The results showed that the greenschist presented time-dependent behaviour under long-term loading. The samples generally experienced two stages: transient creep and steady creep, but no accelerating creep. The periods of transient creep and steady creep increased with increasing stress levels. The long-term strength of the greenschist was identified based on the variation of creep strain and creep rate. The ratio of long-term strength to conventional strength was around 80% and did not vary much with confining pressures. A quantitative method for predicting the failure period of greenschist, based on analysis of the stress–strain curve, is presented and implemented. At a confining pressure of 40 MPa, greenschist was predicted to fail in 5000 days under a stress of 290 MPa and to fail in 85 days under the stress of 320 MPa, indicating that the long-term strength identified by the creep rate and creep strain is a reliable estimate.

Keywords: greenschist; hard rock; creep behaviour; creep stage; creep rate; long-term strength

1. Introduction

Rock is a complex and heterogeneous geological material which includes various defects that can lead to time-dependent behaviour. Creep is defined as the time-dependent deformation of rock under a load that is lower than the short-term strength of the rock (Shin *et al.* 2005). Creep is a fundamental mechanical characteristic of rock and is essential for evaluation of long-term stability of underground structures. Therefore, the study of rock creep is an important research field in rock mechanics and rock engineering (Zhou 2011). Laboratory testing is the main method used to investigate the time-dependent properties of rock. Many experimental and theoretical studies were

*Corresponding author, Professor, E-mail: bajang@kangwon.ac.kr

performed to describe the creep behaviour of rocks and valuable results were obtained (Boukharov *et al.* 1995, Fujii *et al.* 1999, Jin and Cristescu 1998, Fabre and Pellet 2006, Sterpi and Gioda 2009, Wang *et al.* 2014, 2015).

Over the past two decades, many large-scale hydropower station projects were constructed in hard rock in southwest China. Due to the special geological environment in this region, the rocks in these projects often exhibit continuous creep deformation, indicating that the deformation is not only large, but also time-dependent (Wang *et al.* 2006). Measurements in newly completed underground caverns show that the deformation of some critical areas in the surrounding rock is still increasing one year after the completion of the project and showing no tendency of convergence (He and Xie 2005). This phenomenon illustrates the long-term viscous behaviour of hard rock, where progressive damage can occur after stress redistribution. Furthermore, creep deformation has led to the failure of some rock bolts (Zhu *et al.* 2011). Therefore, the creep behaviour of hard rocks in these projects should be thoroughly investigated for long-term stability evaluation.

In previous studies, it was generally believed that hard rock does not have very obvious creep behaviour in practical engineering. Creep deformation in hard rock tends to be significantly less than that in soft rock (Malan 1999). However, some experimental results have shown that hard rock can also exhibit time-dependent deformation under relatively high-stress conditions (Miura *et al.* 2003). An in-situ creep test on hard rock showed that both elastic strains and creep strains could be observed (Korzeniowski 1991). Further investigations were carried out to study the creep properties of hard rock (Malan 2002, Zhang *et al.* 2013). During the creep process of hard rock, three distinct stages can be observed: transient creep, steady creep and accelerating creep (Boukharov *et al.* 1995). The period of transient creep, during which the creep rate decreases continually with time, usually depends on the applied stresses (Xu *et al.* 2006). In the steady creep stage, the strain rate is almost constant with time, and finally, during the accelerating stage, the creep rate increases significantly. Depending on the loading conditions, any one of the three stages described above may dominate the deformation process. The transient creep and steady creep stages can often be observed, but the accelerating creep can be difficult to detect and therefore is less frequently observed (Wang 2004).

Test results have shown the existence of a stress threshold during the creeping of rock (Zhang *et al.* 2012, Yang *et al.* 2014). When the applied load is below the stress threshold, only transient creep and steady creep appear and the viscoplastic deformation can be stabilized over a long time (Cui and Fu 2006). The steady creep rate is low when the stress level is lower than this stress threshold. This indicates that microcracks have formed but the stress is not high enough to develop further cracks in the rock (Fabre and Pellet 2006). However, when the applied load is above the stress threshold, steady creep with a high strain rate or an accelerating creep will develop. The steady or accelerating creep can lead to coalescence and interaction of microcracks and final failure of the rock (Sangha and Dhir 1972). This stress threshold is usually defined as the long-term strength of the rock. Methods to identify the long-term strength of rock were reported by some researchers (Lajtai 1991, Liu and Xu 2000, Zhang *et al.* 2011). These methods can be classified as direct methods and indirect methods. Direct methods attempt to determine the stress threshold under which the rock mass does not fail in a predefined period of time. Indirect methods aim to identify the critical strength or criterion for different stages of creep under external loading by observing the physical phenomena in the rock (Munday *et al.* 1977). Pushkarev and Afanasev (1973) proposed a relaxation method to determine the long-term strength of rock. In this method, continuous cyclic loading and relaxing were performed and the long-term strength was determined

from the stabilized maximum relaxation stress. The long-term strength of a rock can also be determined by identifying the transition point from stable to unstable crack propagation (Bieniawski 1967), i.e., the turning point on the volumetric stress–strain curve. Although there have been some endeavours to investigate the long-term strength of rock and to solve the creep mechanics problems encountered in rock engineering, our knowledge is not sufficient to accurately describe the time-dependent characteristics of hard rock. Further investigations are required to reliably evaluate the long-term strength properties of rock.

In this paper, a series of laboratory tests were carried out to study the time-dependent characteristics of greenschist samples collected from the construction site of the Jinping II hydropower station. The creep properties of greenschist under different loading conditions were investigated and used to estimate the long-term stability and safety of the hydropower station. Uniaxial and triaxial compressive conditions were selected to evaluate the deformation mechanism, failure process, and time-dependent changes of greenschist under long-term loading. Emphasis was placed on the investigation of the creep behaviour of hard rock and on the method for determining long-term strength during the creep process. Finally, a novel method for quantitatively analyzing the long-term strength of greenschist was proposed and implemented.

2. Preparation and mechanical properties of the samples

The Jinping II hydropower station is located at the Great Jinping River Bend of the Yalong River in Liangshan, Sichuan Province of China (Zhu *et al.* 2011). An important part of the station is the diversion tunnel which is generally 1500–2000 m deep with a maximum depth of 2500 m (Chen *et al.* 2014). A field stress of 40–45 MPa was measured at the construction site. Greenschist commonly appeared during tunnel excavation. Even though these rocks were hard and compact with void cementation, a great deal of time-dependent deformation developed after excavation. For our laboratory test, greenschist cores were taken from intact blocks in the auxiliary access tunnel which was about 1600 m below the surface. The drilled cores were 110 mm in diameter. They were wrapped in protective film and placed in a special box to prevent damage during transport. In the laboratory, all the cores were processed into cylindrical samples 100 mm long and 50 mm in diameter according to ASTM requirements for creep tests (ASTM 2008). The two end faces of each sample were polished smooth. The lithology showed that the greenschist samples were composed mainly of diopside, epidote, garnet, actinolite and chlorite with a few quartz, calcite and schistose structures with grey marble bands and lenses. Rock anisotropy associated with various foliation characteristics can influence the compressive strength of schist rock significantly (John and Maurice 1989, Li *et al.* 2012). Generally, the compressive strength of rock samples with transverse and longitudinal foliation planes was the highest (Donath 1964). For the tests in this study we selected all samples with transverse foliation planes; hence, the rock anisotropy associated with foliation plane orientation was not considered for the test results.

To understand the initial properties of the greenschist, twenty five samples were selected for the laboratory tests. The physical-mechanical parameters, density (ρ), ultrasonic velocity (V_s , V_p), dynamic Poisson's ratio (ν_d) and dynamic elastic modulus (E_d), were obtained according to the ISRM method (ISRM 1981) (Table 1). The coefficient of variation (CV) was used to assess the uncertainty of the parameters. The low CV values in Table 1 indicate that the greenschist samples were relatively uniform and of high integrity.

To confirm the multi-step stress levels for the creep tests, the short-term strength and

Table 1 Physical-mechanical properties of greenschist

| ρ (g/cm ³) | | V_s (m/s) | | V_p (m/s) | | v_d | | E_d (GPa) | |
|-----------------------------|--------|-------------|--------|-------------|--------|---------|--------|-------------|--------|
| Average | CV (%) | Average | CV (%) | Average | CV (%) | Average | CV (%) | Average | CV (%) |
| 2.71 | 0.42 | 1494 | 2.15 | 2497 | 1.97 | 0.22 | 7.8 | 14.74 | 5.67 |

Table 2 Results of the uniaxial compression tests for greenschist samples

| Sample No. | Uniaxial compressive strength (MPa) | Elastic modulus E (GPa) | Poisson's ratio ν |
|------------|-------------------------------------|---------------------------|-----------------------|
| 1 | 125.7 | 9.37 | 0.24 |
| 2 | 133.6 | 8.59 | 0.26 |
| 3 | 140.2 | 9.90 | 0.25 |
| 4 | 118.7 | 10.20 | 0.25 |
| Average | 129.6 | 9.52 | 0.25 |

Table 3 Results of the triaxial compression tests for greenschist samples

| Sample No. | Confining pressure (MPa) | Triaxial compressive strength (MPa) |
|------------|--------------------------|-------------------------------------|
| 1 | 5 | 155 |
| 2 | 10 | 205 |
| 3 | 10 | 193 |
| 4 | 15 | 221 |
| 5 | 40 | 353 |
| 6 | 40 | 337 |

deformation behaviour of the samples were measured by uniaxial and triaxial compression tests. The results from the short-term tests provided the basis for formulating the creep test program. Four samples were used for the uniaxial compression tests. The tests were performed by increasing the stress on the samples at a constant rate of 0.76 MPa/s. The strains were measured by electric resistance strain gauges. Typical values of the mechanical properties are given in Table 2. The average values of the uniaxial compressive strength, elastic modulus and Poisson's ratio were 129.6 MPa, 9.52 GPa and 0.25, respectively. The confining pressures in the triaxial compression tests were 5, 10, 15, and 40 MPa with a loading rate of 0.05 MPa/s. The compressive strengths under these confining pressures are listed in Table 3. Most samples showed plane shear failure, rather than cone shear failure. The compressive strengths increase with confining pressures. Based on the linear Mohr–Coulomb (MC) criterion, the cohesion of the greenschist samples was 31.2 MPa and the friction angle was 42.3°. The compressive strengths under the confining pressures of 10 MPa and 40 MPa were calculated from the MC criterion as 193.02 MPa and 346.63 MPa, respectively.

3. The creep test program

Two types of creep tests were adopted for this study. Uniaxial creep tests were performed in the National Key Laboratory in Tongji University and triaxial creep tests were performed in the

Yangzi River Scientific Research Institute in Wuhan. Multi-level loading on a single sample was applied since a single-step loading on several samples requires more rock samples and may cause more scatter in the test data. From an initial low value, each sample was loaded to different stress levels by increasing the stress stepwise after a certain time interval for creeping.

A CSS-1950 servo-controlled rheological testing device, made by Changchun Testing Machine Research Institute in China, was used for the uniaxial creep test (Fig. 1). The maximum compressive load for the vertical axis was 500 kN. The stress was measured using a 1.0 MN capacity load cell. The axial strain was measured using two linear variable displacement transducers (LVDT). The samples were placed between the top and bottom platens after fixing the LVDTs to it. Generally, the precision of the displacement measurement was 1 μm . The strain was calculated by averaging the two measurements.

The uniaxial creep test was performed at constant temperature and humidity. The temperature was controlled at $20 \pm 1^\circ\text{C}$ and the relative humidity was maintained at $50 \pm 2\%$ to eliminate any effect of temperature and moisture fluctuation on either the sample or the equipment. The axial



Fig. 1 CSS-1950 biaxial rheological testing device used for the uniaxial creep test



Fig. 2 TLW-2000 triaxial rheological testing device used for the triaxial creep test

load was initially loaded to approximately 50% of the uniaxial compressive strength, and then additional axial loads were applied using a stepwise procedure. The loading rate was 0.13-0.17 MPa/s. Nine stress levels ranging from 58 MPa to 136 MPa were performed. The increment of each stress level was about 10 MPa and each loading was maintained for 72 hours. If the sample did not fail in the predefined time duration, the stress level was increased to the next level until failure.

The triaxial creep tests were performed with the TLW-2000 triaxial rheological testing system (MTS) with a stiff servo-controlled hydraulic test frame, made by Chaoyang Test Instrument Co., LTD, in China (Fig. 2). Confining pressure was supplied using a gas over oil pressure intensifier and controlled by two hydraulic pumps. The axial loading capacity was 2000 kN, and the maximum confining pressure could be controlled at 50 MPa. The axial and lateral strains were measured by four LVDTs and the measurement error was controlled within 1%.

The triaxial creep tests were conducted in a special laboratory, where the room temperature was kept constant at $20 \pm 0.5^\circ\text{C}$. The sample was wrapped with a high-performance plastic cover to protect it against oil penetration and placed in a pressure chamber. The axial stress was applied by a multi-level procedure at a loading rate of 0.1 MPa/s. The axial stress level started from approximately 50% of the calculated triaxial compressive strength. The triaxial creep tests were performed under confining pressures of 10 MPa and 40 MPa. The confining loading was applied at a rate of 0.5 MPa/s by an oil hydraulic system to the predefined hydrostatic state. Each deviatoric stress was kept constant for about 72 hours. Data recording was stopped and the test ended when the rock sample became unstable.

4. Creep test results

4.1 Uniaxial creep test

The test durations, stress levels and creep strains for the uniaxial creep test are summarized in Table 4. The total axial creep strains increase with increasing stress levels. The increasing magnitude is relatively small up to the stress level of 117 MPa. As the stress rises above 117 MPa, the axial creep strains start to increase rapidly. When reaching the final stress level of 136 MPa, the creep strains develop extremely fast, and the sample succumbs to creep failure. The creep strain developed at 136 MPa is even greater than the instantaneous elastic strain.

The complete strain–time curve of the uniaxial creep test is illustrated in Fig. 3(a). The axial strain increased at stepwise intervals and instantaneous elastic strains are followed by creep strains after each loading. The creep curves under various stress levels exhibit similar behaviour; however, the creep strain response is more distinct at the high stress levels of 126 MPa and 136 MPa, especially at 136 MPa where a very clear upward section appears in the strain–time curve. The final failure of the sample was powerful and instantaneous rather than a progressive increase in the rate of deformation. This behaviour was mainly due to the dominant failure mode of sample – brittle damage.

Typical strain-time curves for the stress levels of 68 MPa, 107 MPa and 136 MPa are given in Figs. 3(b)-(d), respectively. Both transient creep and steady creep are clearly observed but accelerating creep is absent. Transient creep is considered as the initial creep with a nonlinear relation with time. Timoshenko (1953) stated that transient creep is essentially caused by the elastic aftereffect in the sample and the period of transient creep varies for different loading

conditions. The test results in this study show that the durations of transient creep tend to increase as the stress levels become larger. A special case is at the highest stress level (136 MPa) where the duration of the transient creep was shortest, indicating that the stress level was sufficiently high to exceed the crack damage threshold. The transition from transient creep to steady creep indicates that the elastic limit has been exceeded and the sample is softening (Ma and Daemen 2006). The steady creep stages lasted longer than the transient creep stages at each stress level. Most of the steady creep intervals lasted more than 40 hours. During the steady creep stages, the strains increased approximately linearly with time; therefore, the slopes of the straight lines may be considered as the steady creep rates (Fig. 3). These slopes are clearly steeper under larger stress levels.

The creep rates were obtained by calculating the slope of the strain–time curves (Fig. 4). As soon as the stresses are applied, the creep strains develop at a high initial rate and then decrease rapidly and tend to stabilize at a relatively constant value over time. Some equations, such as exponential functions and power functions, were proposed to describe the creep rate versus time relationships (Cruden 1971, Yang *et al.* 1999, Ma and Daemen 2006). The tendency of the creep rate described in these equations is very similar to that in our study. The point where the strain rate stabilizes marks the end of the transient creep and the beginning of the steady creep. The steady creep rates for the low stress levels of 68 MPa and 107 MPa are relatively small; however, at 126 MPa, the steady creep rate becomes larger. Thus, the steady creep rates increase with increasing stress levels, rising to very high rates at the final stress of 136 MPa.

For engineering applications it is very important to know when steady creep was reached and the magnitude of the steady creep rate (Yang *et al.* 1999). The circles in Fig. 4 represent the transition of the strain rates between the transient and steady creep stages at different stress levels. The points at which the creep rates become approximately constant are chosen as the boundaries between the two creep stages. The length of the transient creep phase was identified as 14 hours, 20 hours, 30 hours and 6 hours under the stress levels of 68 MPa, 107 MPa, 126 MPa and 136 MPa, respectively. Fig. 5 gives the durations of the transient creep at different stress levels. An exponential function ($y = 6.6217e^{0.0112x}$) can describe the relationship between the duration of the transient creep phase and the stress levels. The function indicates that under larger stress levels, the creep will take longer to stabilize. It should be noted that when the first stress level of 58 MPa was applied, the primary micro-fissure in the sample gradually closed, resulting in a pretty long period of transient creep. When the last stress level of 136 MPa reached, the macroscopic damage

Table 4 Results of the uniaxial creep test

| Axial stress (MPa) | Test durations (hour) | Total axial creep strain ($\mu\epsilon$) |
|--------------------|-----------------------|--|
| 58 | 71.2 | 108 |
| 68 | 69.8 | 114 |
| 77 | 70.6 | 118 |
| 87 | 69.4 | 128 |
| 98 | 71.2 | 140 |
| 107 | 68.9 | 146 |
| 117 | 70.2 | 152 |
| 126 | 71.4 | 224 |
| 136 | 13.5 | 330 |

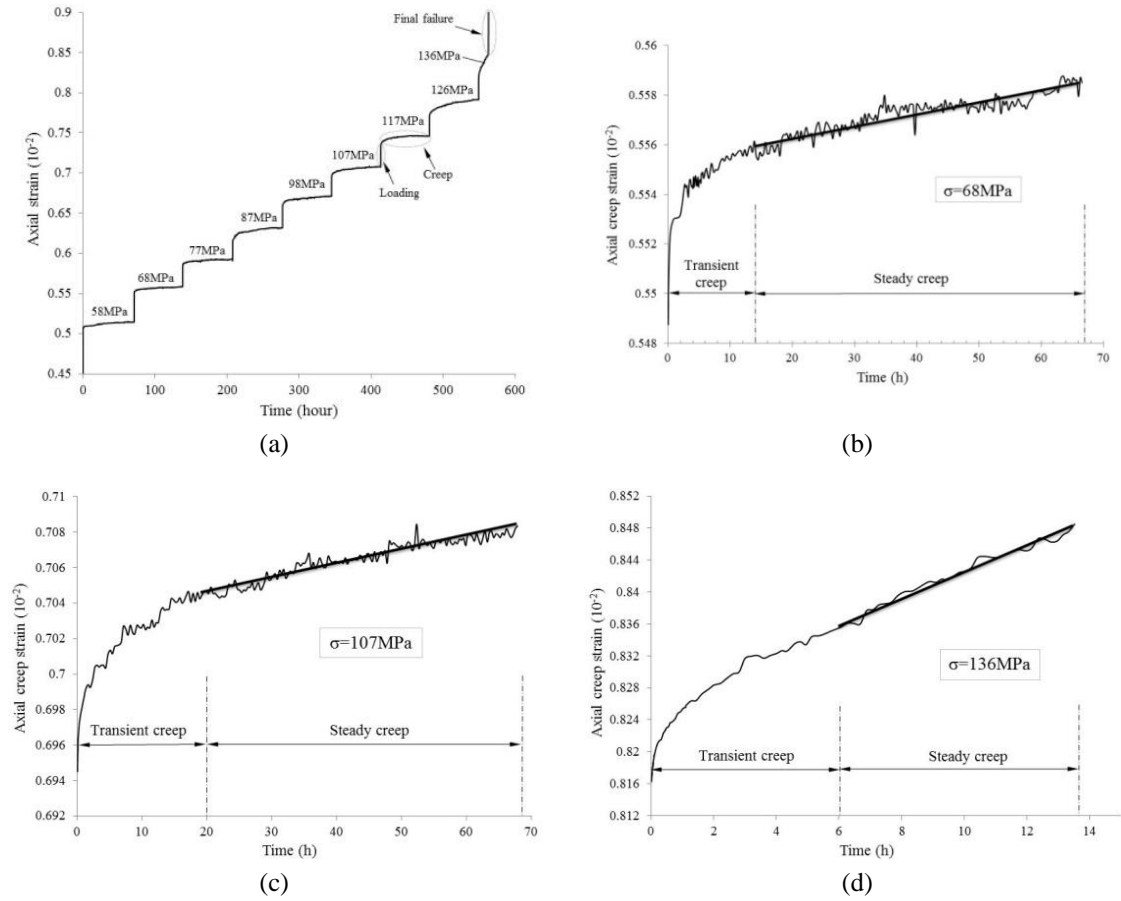


Fig. 3 (a) Complete strain–time curve for the uniaxial creep test and strain–time curves; (b) under 68 MPa; (c) under 107 MPa; and (d) under 136 MPa

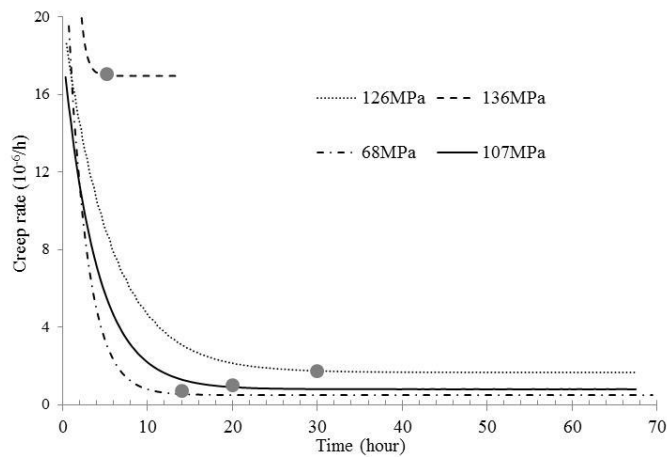


Fig. 4 Axial creep rate over time under stress levels of 68 MPa, 107 MPa, 126 MPa and 136 MPa. The circles indicate the transition points from the transient creep stage to the steady creep stage

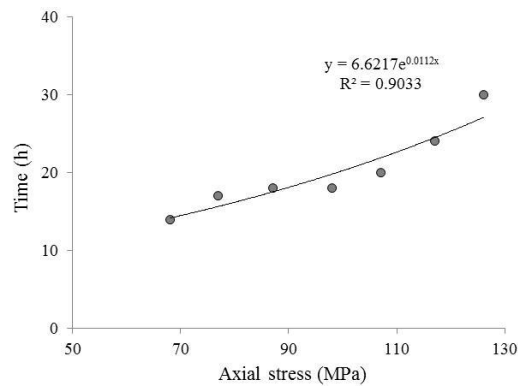


Fig. 5 Duration of transient creep under different stress levels. The relationship of duration of transient creep versus stress level can be described by an exponential function

occurred, and the sample experienced the shortest period of transient creep. Thus, the periods of transient creep at the initial and final stress levels were not considered in the function for their special cases.

4.2 Triaxial creep test

Table 5 presents the test durations, stress levels and creep strains for the triaxial creep tests. Both the axial and lateral creep strains increase with rising axial stress levels. At the confining pressure of 10 MPa, the increase in axial creep strain is more pronounced at stress levels above 160 MPa. The lateral creep strain has a same tendency, but its magnitude is greater. Similar behaviour can be seen at the confining pressure of 40 MPa. When the stress level is above 290 MPa, the axial strain starts to increase more rapidly. The axial creep strain under the final stress level is almost eight times larger than that under the initial stress level. The lateral creep strains increase much faster than the axial creep strain when the rock sample is close to failure.

Typical results of time-dependent evolution of the axial, lateral and volumetric strains at different confining pressures are shown in Fig. 6. The creep strains at the confining pressure of 10 MPa and 40 MPa exhibit similar behaviour; the axial strains and lateral strains increase stepwise with time. The creep behaviour is more pronounced in the lateral direction than in the axial direction. The strain plots show typical transient and steady creep behaviour but no accelerating creep. Yang *et al.* (1999) showed that the transient creep of salt rock decreased with increasing confining pressures. Chen *et al.* (2014) suggested that the transient creep of marble depends on deviatoric stress more than on the confining pressure. In this study, we cannot directly compare the transient creep strains with respect to confining pressures, because the creep data were collected under different magnitudes of axial stress levels. Some authors expressed doubts as to the existence of the steady creep stage during triaxial creep tests performed on hard rock since they did not observe the stabilization of strain rates (Dusseault and Fordham 1993). However, the results of our greenschist tests clearly show the steady creep phase, with higher steady creep rates at high stress levels (Fig. 7). The length of the steady creep phase is clearly longer than that of the transient creep phase. The steady creep leads to an increase in creep strains with time until the final rock failure. Both samples were observed to fail suddenly, immediately after the last increase of axial stress.

The development of axial and lateral strains varies under different loading conditions. At confining pressures of 10 MPa, the axial strains are larger than the lateral strains under initial low stress levels. The samples show mainly volumetric compression with smaller lateral dilatancy (Fig. 6). With increasing stress levels, the lateral strains develop rapidly and gradually exceed the axial strains. As the stress levels rise, the lateral strains become dominant, resulting in rapid volumetric expansion. When the rock samples rupture, the lateral strain is much higher than the axial strain. Several studies found similar behaviour in triaxial creep tests (Liu *et al.* 2006, Zhang *et al.* 2013, Yang *et al.* 2014). Cui and Fu (2006) showed that the lateral strains were more dominant than the axial strains during triaxial creep tests, which indicates that micro-cracks developed with time and a large number of new cracks were generated. The creep strains obtained in our tests (Table 5) are consistent with those of previous studies.

The volumetric expansion is mainly due to the propagation of microcracks and is usually related to the deviatoric stress and time (Zhang *et al.* 2012). The volumetric creep strains shown in Fig. 6 can be divided into compression and dilatation stages. At low stress levels, the volumetric strain shows compressive behaviour; as the deviatoric stresses and time increase, the volumetric strains also increase. With continued loading, the volume reverses from compression to dilatation. At the final stage, the volumetric expansion is quite severe. At a confining pressure of 40 MPa, the sample showed dilating behaviour as soon as the first stress level was applied. This is because the lateral strain was large when the load was applied. As the deviatoric stresses increased further, the lateral expansion became greater and greater. The volumetric strain curve does not exhibit a clear compression stage. Generally, however, the tendencies of the volumetric strains under the two confining pressures are similar.

Table 5 Results of the triaxial creep tests

| Confining pressure (MPa) | Axial stress (MPa) | Test durations (hour) | Axial creep strain ($\mu\epsilon$) | Lateral creep strain ($\mu\epsilon$) |
|--------------------------|--------------------|-----------------------|--------------------------------------|--|
| 10 | 90 | 73.2 | 47 | 50 |
| | 105 | 71.1 | 48 | 55 |
| | 120 | 72.5 | 61 | 128 |
| | 140 | 71.7 | 105 | 160 |
| | 160 | 72.3 | 107 | 212 |
| | 180 | 71.8 | 194 | 253 |
| | 190 | 71.3 | 343 | 558 |
| 40 | 150 | 71.8 | 136 | 156 |
| | 170 | 72.2 | 110 | 52 |
| | 190 | 71.6 | 221 | 93 |
| | 210 | 71.4 | 237 | 258 |
| | 230 | 72.1 | 237 | 380 |
| | 260 | 71.2 | 320 | 694 |
| | 290 | 71.8 | 385 | 1046 |
| | 320 | 70.0 | 502 | 2263 |
| 350 | 72.5 | 893 | 4496 | |

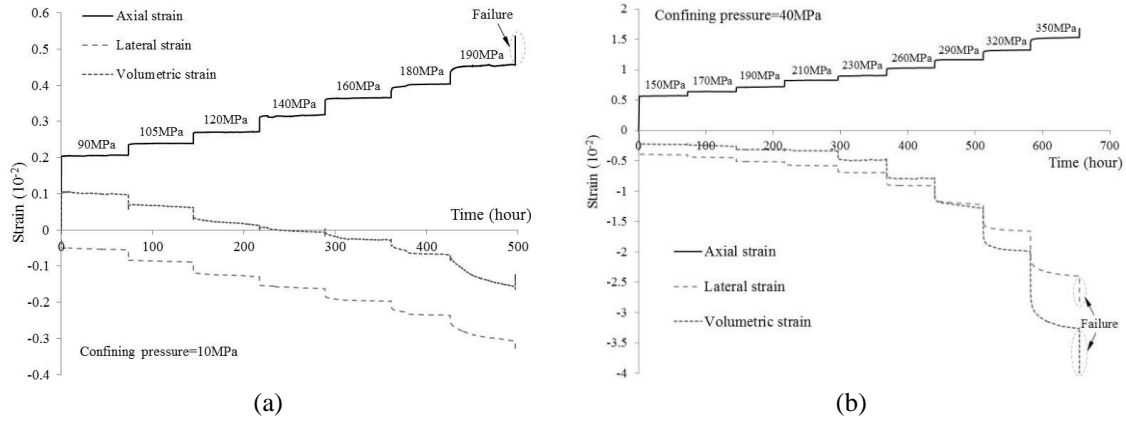


Fig. 6 Complete strain–time curves for the triaxial creep tests (a) with a confining pressure of 10 MPa; and (b) with a confining pressure of 40 MPa

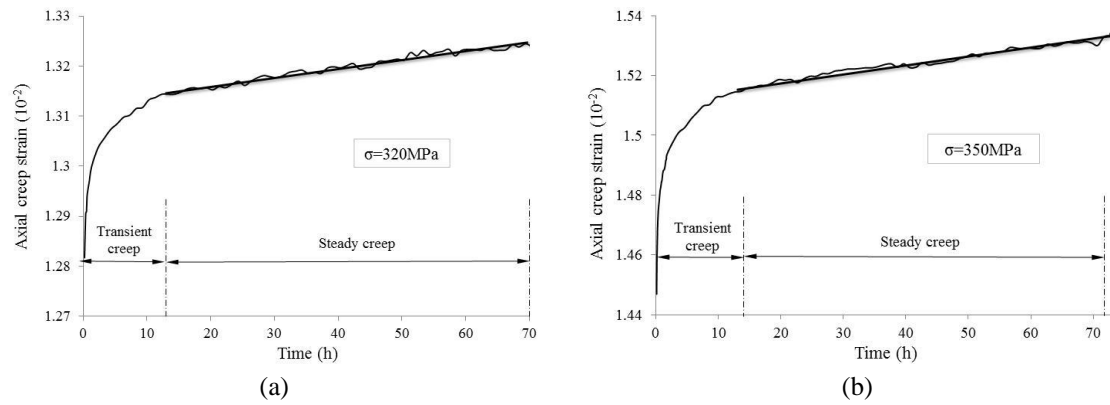


Fig. 7 Strain–time curves under axial stress levels of (a) 320 MPa; and (b) 350 MPa with a confining pressure of 40 MPa

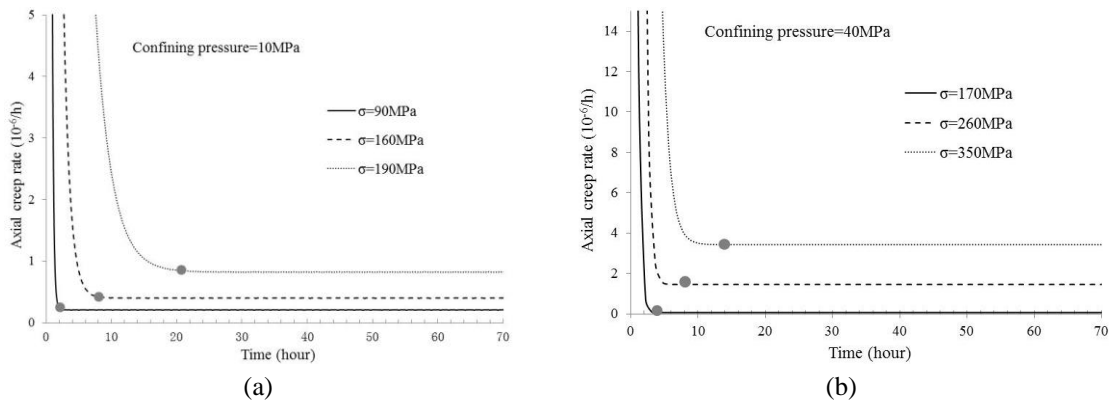


Fig. 8 Axial creep rate over time under different stress levels during the triaxial creep tests. Curves of creep rate with (a) confining pressure of 10 MPa; and (b) confining pressure of 40 MPa. The circles represent the transition points from the transient creep stage to the steady creep stage

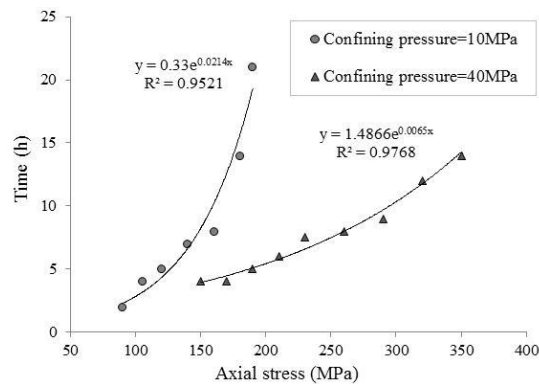


Fig. 9 Duration of transient creep under different deviatoric stress levels. The relationships of durations of transient creep versus stress level can be described by exponential functions

The axial creep rates at different stress levels are shown in Fig. 8. The behaviour of the creep rate under different loading conditions is similar. The circles mark the transition points from transient creep to steady creep. The periods of transient creep stage were longer with increasing deviatoric stresses. Results from Liu and Xu (2000) and Chen *et al.* (2014) also showed that the time needed for the creep rates to stabilize clearly increased with deviatoric stress levels under different constant loading conditions. Therefore, we conclude that the length of the transient creep stage depends on the deviatoric stress levels. Moreover, the steady creep rates increase when the deviatoric stresses are higher. Previous studies suggest that the steady creep rates usually increase with increasing deviatoric stresses, but decrease with increasing confining pressures (Yang *et al.* 1999, Ma and Daemen 2006, Zhang *et al.* 2015). Since the applied axial loadings in our tests were different, we did not directly compare the steady creep rates with different confining pressures, but we note that most of the steady creep rate values at the confining pressure of 10 MPa are lower than those at the confining pressure of 40 MPa. This may be explained by the fact that most of the deviatoric stresses are larger at the confining pressure of 40 MPa.

Using the transition point for creep rates at different stress levels, the times of the transition between transient creep and steady creep were identified (Fig. 9). Under different confining pressures, the durations of transient creep show a similar tendency, an exponential increase of the transition point as the stress levels rise, indicating that the larger the deviatoric stress on the sample, the longer the time it will take to reach the steady creep stage. Under different confining pressures, the time to reach steady creep is similar at the initial stress levels, but the rate of increase at the confining pressure of 10 MPa is greater than that at the confining pressure of 40 MPa.

5. Determination of long-term strengths

5.1 Long-term strength determination by uniaxial creep test

The long-term strength of rock is the stress above which the growth, coalescence and interaction of microcracks becomes unstable. Above the long-term strength, the relationship between the applied stress and crack growth velocity will control the propagation process of unstable cracks. Under such conditions, crack propagation will continue until failure even if the

applied loading is constant (Miura *et al.* 2003). Costin (1985) stated that if the stress applied exceeds the long-term strength, damage will continue to develop, resulting in an accelerated strain rate and failure. Martin and Chandler (1994) suggested that the long-term strength for brittle rock could be given by the crack damage stress threshold, above which rock failure would occur if the stress was applied long enough. During the creep process, the crack growth velocity is shown as strain rate, especially the strain rate at the steady creep stage. Chen *et al.* (2014) reported that when the applied load exceeds the long-term strength, the steady creep rate increases rapidly with increasing stresses and the creep strains also rise. The accumulation of creep damage will lead to the development of numerous unstable cracks and rock failure. Therefore, the stress level at which the steady creep rate and creep strain begin to increase rapidly can be identified as the long-term strength.

The steady creep rates under various stress levels applied in the uniaxial creep test are illustrated in Fig. 10. The steady creep rates are small ($0.42\text{--}0.92\ \mu\epsilon/\text{h}$) and increase slightly below the stress level of 117 MPa. Above 117 MPa the creep rates start to increase rapidly. At stress levels of 126 MPa and 136 MPa, the steady creep rates increase to $3.75\ \mu\epsilon/\text{h}$ and $16.97\ \mu\epsilon/\text{h}$, respectively. The higher stress levels clearly lead to larger steady creep rates, and the inflection point is about 117 MPa. The total creep strains at various stress levels are also given in Fig. 10. Since the loading durations are different at each stress level, the durations of each stress level have been normalized for 72 hours by extrapolation. The total creep strains also increase slowly with stress levels up to 117 MPa, but increase rapidly above 117 MPa. Therefore, the stress of 117 MPa was determined as the crack damage threshold, and the long-term strength of greenschist under uniaxial compression may be identified as about 117 MPa.

The sample failed at the stress level of 136 MPa. Although the failure strength obtained in a uniaxial creep test is usually lower than that by a conventional uniaxial compression test (Zhang *et al.* 2011), the failure strength determined by the uniaxial creep test is slightly higher than the average uniaxial compressive strength (see Table 2). The difference may be caused by the 10-MPa increase in stress level or by the inhomogeneity of the rock samples. This indicates that the failure strength may be lower than the 136 MPa obtained by the creep test. Therefore, the long-term strength may be estimated as around 80% of the uniaxial compressive creep strength. This implies

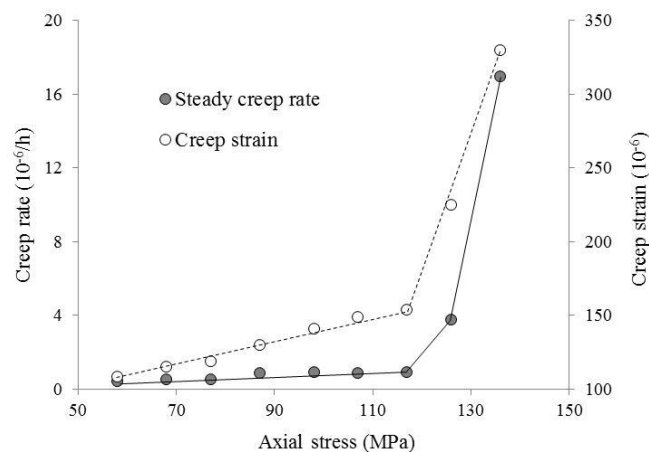


Fig. 10 Steady creep rates and total creep strains along the axial direction from the uniaxial creep test

that the reduction in the overall time effect on the rock strength is approximately 20%. This finding was supported by Lajtai (1981) through tests on granite samples. Martin and Chandler (1994) suggested that the crack damage stress at which a sample will eventually fail under prolonged loading should be about 70-80% of the peak sample strength. The long-term strength obtained for greenschist in this study is within this range.

5.2 Long-term strength determination by triaxial creep test

A similar process to that of the uniaxial creep test was carried out to obtain the long-term strength by triaxial creep tests. Cui and Fu (2006) carried out triaxial creep tests to identify the long-term strength of sandstone by observing the development of axial and lateral creep, and suggested that when evaluating the long-term strength, lateral creep behaviour should be considered for its sensitivity. Our results show that the development of lateral creep has a similar tendency to that of axial creep but the magnitude is usually greater. Thus, the long-term strengths from the triaxial creep tests were identified by considering both the axial and lateral creep.

Fig. 11 shows the steady creep rates under different stress levels at a confining pressure of 10 MPa. The axial and lateral steady creep rates have low values at the initial stress levels and increase slightly with increasing stresses up to 160 MPa. For stresses above 160 MPa, the lateral creep rates increase faster and become larger than the axial creep rates. The inflection point for lateral creep rate is identified as 160 MPa. However, the axial creep rates increase slightly with rising stress levels and do not exhibit a sharp inflection point until the axial stress reaches 180 MPa. The axial and lateral creep strains under different stress levels are shown in Fig. 12. The lateral creep strains are greater than the axial creep strains for all stress levels but increase sharply when reaching 180 MPa. The axial creep strains increase faster when the stress rises above 160 MPa; thus, the inflection point for the axial creep strain is 160 MPa. Taking into account engineering safety factors and the creep in both the axial and lateral directions, the long-term strength can be identified as the lower stress level of 160 MPa at a confining pressure of 10 MPa.

The steady creep rates under different axial stress levels at a confining pressure of 40 MPa are given in Fig. 13. Both the axial and lateral steady creep rates increase slowly with rising stress levels up to 290 MPa. Above 290 MPa the axial and lateral creep rates increase more rapidly, but at a different rate. Thus, the inflection point for the steady creep rate is identified as 290 MPa. The creep strains under different stress levels exhibit a different tendency (Fig. 14); the lateral creep strains increase greatly when the stress is above 290 MPa, but the axial creep strains have no obvious inflection point. From the results of the steady creep rate and creep strain, we identify the long-term strength as 290 MPa at a confining pressure of 40 MPa.

It is worth noting that the axial and lateral creep strains and strain rates under different stress levels are different. Ma and Daemen (2006) found that in laboratory tests the lateral creep often increased earlier and at a greater rate than the axial creep. This may be explained by the smaller restraint of the sample in the lateral direction compared with the axial restraint in the axial creep test. However, in practical engineering, the lateral restraint can also be very large and sometimes even larger than the axial restraint. Moreover, the axial direction is usually the main stress direction while the lateral direction may be considered as having infinite extension. Therefore, the threshold stress in the axial direction is more reasonable and applicable. In our study, it is sometimes difficult to find obvious inflection points for axial creep, so we identified the long-term strength based on the variation of both the axial and lateral creep. The results show that the long-term strength determined based on the axial and lateral creep is relatively safe.

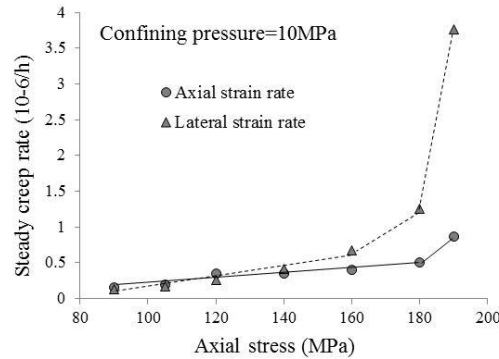


Fig. 11 Axial and lateral steady creep rates from the triaxial creep test with a confining pressure of 10 MPa

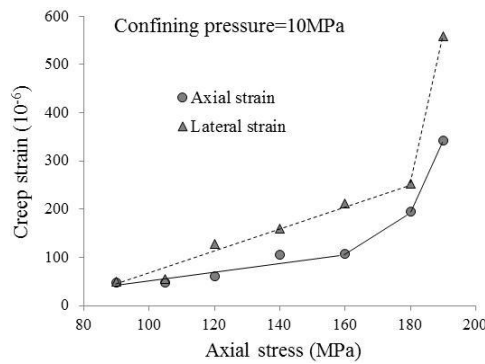


Fig. 12 Axial and lateral creep strains from the triaxial creep test with a confining pressure of 10 MPa

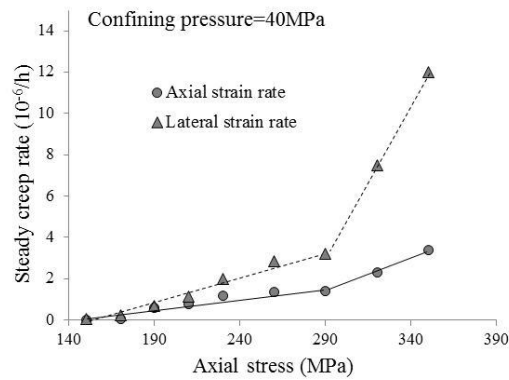


Fig. 13 Axial and lateral steady creep rates from the triaxial creep test with a confining pressure of 40 MPa

The state of uniaxial compression can be thought as that under a confining pressure of zero. According to the analysis in the above sections, the long-term strength for greenschist is identified as about 80% of the conventional strength under three different confining pressures. The confining pressure has no obvious effect on the long-term strength of greenschist. These results are significant and should be further investigated in future research.

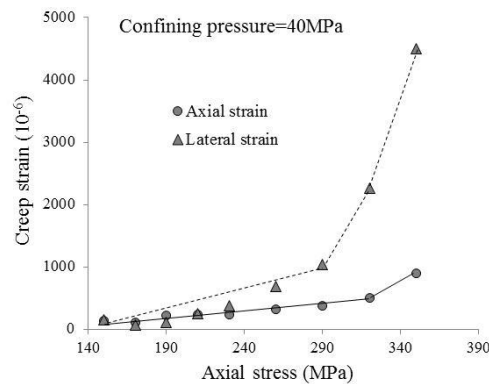


Fig. 14 Axial and lateral creep strains from the triaxial creep test with a confining pressure of 40 MPa

6. Failure predicted by the stress–strain curve of the triaxial compression test

There have been many methods to identify the long-term strength of rock mass; however, each method has its own disadvantages and application limits (Pushkarev and Afanasey1973, Shao *et al.* 2003, Cui and Fu 2006, Yang and Jiang 2009). Some rapid methods are based on insecure foundations or require special conditions to be applied in the tests; therefore, further investigations on long-term properties need to be conducted. It is relatively simple and feasible to determine the long-term strength of rock based on the variations of creep rate and creep strain. The key issue is to find the inflection point during the creep process. However, this approach is often affected by subjective factors and can only determine the long-term strength qualitatively rather than quantitatively.

In general, the stress–strain curves are often used to describe the rock failure process during compression tests. The relation between the stress–strain curve and the creep curve was investigated by Wawersik and Brace (1971), Cruden (1974) and Luo (2008). The studies showed strong evidence that creep failure, at sustained stresses below the peak strength, can lead to failure strains that are closely related to strains observed in the complete stress–strain curve of a conventional test (Hudson 1971, Peng 1973, Ma 2004). This indicates that the strains at failure induced by creep are similar to the strains that would be reached at the same post-peak stress. Therefore, the complete stress–strain curve can help us understand the creep process and predict the creep strains. Fig. 15 shows two pairs of points; each pair has points of equal stress, one at the pre-peak stage of the stress–strain curve and the other at the post-peak stage. Since the rock is already in the failure stage at the post-peak stage, the strain under this stress level at the post-peak stage can be deemed as the critical strain value when rock failure occurs. If we consider another point at the same stress level in the creep test, when the creep strain under this stress level reaches the strain difference between the two points, the rock will fail during creeping.

We selected triaxial test data with a confining pressure of 40 MPa for our analysis (Fig. 15). The strength values were normalized by calculating the ratio of stress to failure strength to eliminate non-uniformity. Two stress levels of 290 MPa and 320 MPa close to the long-term strength were used for the analysis. The strain values and strain differences under the same stress levels in the complete stress–strain curve are given in Table 6. These results can be used to compare the strain differences with the predicted strains in the creep test.

To model the strains under long-term loading, the creep model and the parameters for this model should be identified. In this study, the Burgers model was chosen to describe the creep properties for its widespread applicability (Zhang *et al.* 2015). We calculated the strain in a specified period based on the Burgers model and determined whether the calculated strain exceeds the strain difference according to Table 6; this will predict whether the rock will fail in this specified period.

The equation of the Burgers model is as follows

$$\varepsilon = \sigma_0 \left[\frac{1}{E_M} + \frac{t}{\eta_M} + \frac{1}{E_K} \cdot \left(1 - e^{-\frac{E_K t}{\eta_K}} \right) \right] \tag{1}$$

Eq. (1) describes the standard four-element viscoelastic Burgers model (Fig. 16) subjected to a constant stress (σ_0) for a particular time-period (t). Based on Eq. (1), the corresponding stress–strain with time showing the different phases can be obtained. The model parameter E_M is the elastic coefficient of the Maxwell sub-unit and E_K is the elastic coefficient of the Kelvin sub-unit; η_M is the viscous coefficient of the Maxwell sub-unit and η_K is the viscous coefficient of the Kelvin sub-unit. The model parameters were determined using the back analysis method. We used pattern search and least-square techniques and set the tolerance and initial values of the parameters to be identified. The initial parameters were adjusted until suitable values were obtained. The fitting curves based on the Burgers model are shown in Fig. 17. The parameter values obtained from the fitting results are given in Table 7. By substituting these parameters into the Burgers model (Eq. (1)), the strain values in a specified period can be calculated (Table 8).

Table 6 Strains measured at the pre-peak and post-peak stages for stress levels of 290 MPa and 320 MPa

| Stress level (MPa) | Stress ratio | Axial strain before peak stress ($\mu\varepsilon$) | Axial strain after peak stress ($\mu\varepsilon$) | Strain difference ($\mu\varepsilon$) |
|--------------------|--------------|--|---|--|
| 290 | 77% | 11570 | 16530 | 4960 |
| 320 | 85% | 12740 | 16490 | 3750 |

Table 7 Parameters calculated for the Burgers model

| Stress level (MPa) | Stress ratio | E_M (MPa) | E_K (MPa) | η_M (MPa/H) | η_K (MPa/H) |
|--------------------|--------------|-------------|--------------------|--------------------|--------------------|
| 290 | 77% | 251 | 2.39×10^4 | 7.19×10^7 | 1.35×10^5 |
| 320 | 85% | 247 | 1.70×10^4 | 1.83×10^6 | 5.49×10^4 |

Table 8 Failure strains and times calculated by the Burgers model

| Time (day) | Time (hour) | Strain under 290 MPa ($\mu\varepsilon$) | Strain under 320 MPa ($\mu\varepsilon$) |
|------------|-------------|---|---|
| 0 | 0 | 11550 | 12960 |
| 1 | 24 | 11670 | 13190 |
| 85 | 2040 | 11760 | 16710 |
| 365 | 8760 | 12030 | 28460 |
| 5000 | 120000 | 16520 | 222990 |
| 36500 | 876000 | 47010 | 1545000 |

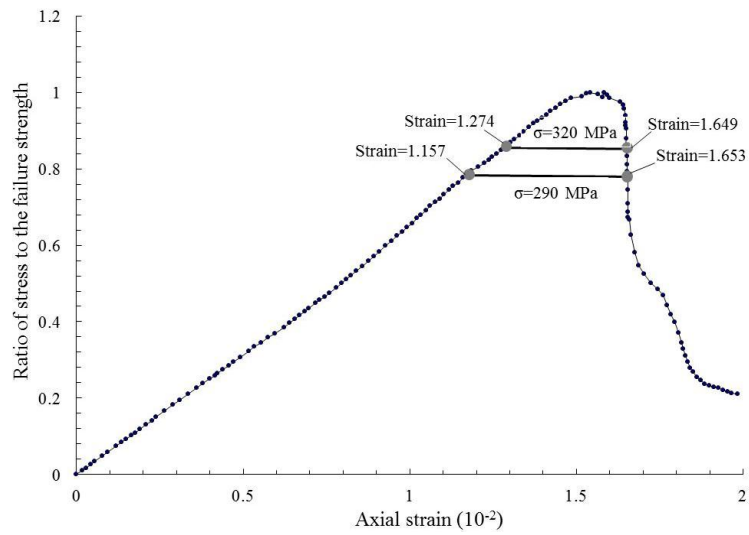


Fig. 15 Ratio of stress to failure strength versus strain curve from the triaxial compression test with a confining pressure of 40 MPa. The strains at the pre-peak and post peak stages are measured for stress levels of 290 MPa and 320 MPa

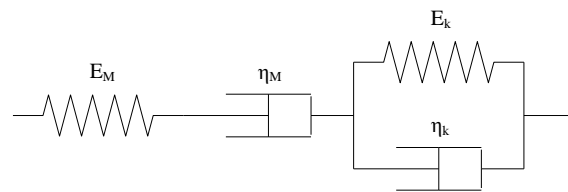


Fig. 16 Schematic illustration of the Burgers model used in this study

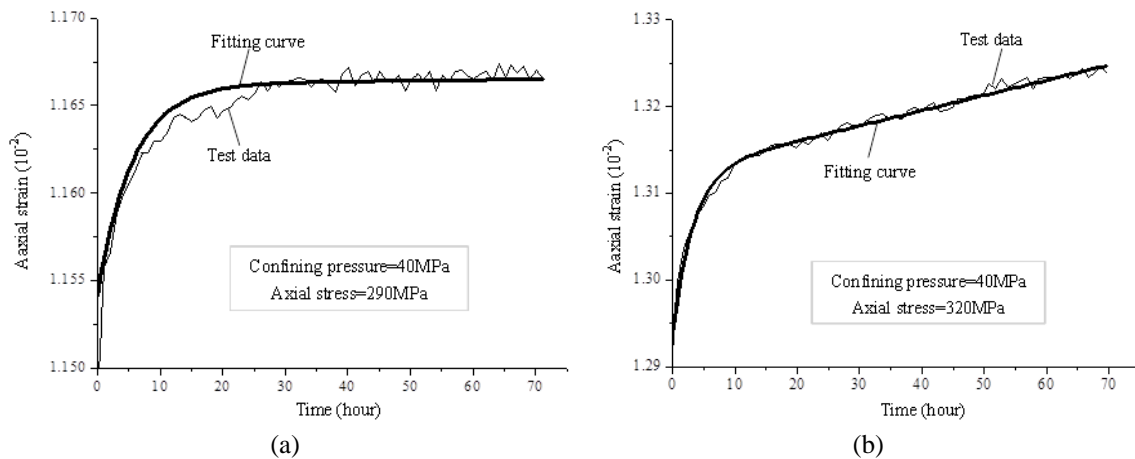


Fig. 17 Axial strain versus time curves measured by the triaxial creep tests and predicted by the Burgers model for creep stresses of (a) 290 MPa; and (b) 320 MPa with a confining pressure of 40 MPa

For $t=0$, the calculated strains under stresses of 290 MPa and 320 MPa should be instantaneous strains: 11550 $\mu\epsilon$ and 12960 $\mu\epsilon$, respectively. Adding the instantaneous strains and the strain differences shown in Table 6, we can obtain the predicted strains at which the rock may fail. The failure strain at stresses under 290 MPa and 320 MPa is 16520 $\mu\epsilon$ and 16710 $\mu\epsilon$, respectively. Table 8 indicates that the greenschist is predicted to fail in 5000 days, i.e. about 13 years under a stress level of 290 MPa. Under a stress level of 320 MPa, the greenschist may fail in 85 days. The time to failure under a stress of 290 MPa is much longer than that under 320 MPa.

The proposed method is capable of quantitative analysis. Based on this method, it is possible to quantitatively estimate the long-term stability of rock considering the stress-strain curve and creep curve together. The method provides a novel means of analyzing the long-term mechanical properties of rock using the pre-peak and post-peak stage of stress-strain curve. Furthermore, the short-term and long-term characteristics of rock could be connected by this method in future research. However, the critical load is highly related to the measuring accuracy of the test facility, especially the accuracy of the strain measurement. Although the accuracy of the data obtained through the current method and testing device is limited, it nevertheless provides a novel method for quantitatively analysing the long-term strength of a rock sample.

7. Conclusions

To investigate the time-dependent behaviour and long-term strength of greenschist, a series of uniaxial and triaxial creep tests were performed. Based on experimental data, the transient and steady creep behaviour of the samples was analysed in detail. The long-term strength of greenschist was identified based on the variation of creep rates and creep strains. A quantitative method was proposed to further investigate the long-term characteristics. The following conclusions were drawn from this study.

- The creep tests show that the greenschist can present time-dependent behaviour at various stress levels. During the creep process, the rock sample generally experiences transient creep and steady creep but does not show accelerating creep. Both the creep strains and steady creep rates increase with increasing stress levels. The transition points between the transient creep and steady creep show that the period of transient creep also increases with rising stress level.
- The long-term strength of greenschist may be determined by steady creep rates and creep strains. According to the stress threshold obtained in our analysis, the ratio between the long-term strength and conventional strength does not vary much with confining pressure. The long-term strength is around 80% of the conventional strength.
- A quantitative analysis method based on the stress-strain curve is proposed in this study to quantitatively estimate the long-term stability of rock. The method provides a novel means of quantitatively analysing the long-term strength properties of the rock. The calculated results at a confining pressure of 40 MPa show that the long-term strength identified by creep rate and creep strain is in agreement with previous estimates.

Acknowledgments

This work is supported by The National Basic Research Program of China – Program 973 (Grant No. 2014CB046905) and a grant from the Energy Efficiency & Resources of the Korea

Institute of Energy Technology Evaluation and Planning (KETEP) funded by the Korean government's Ministry of Knowledge Economy.

References

- ASTM D7070-08 (2008), Standard Test Method for Creep of Rock Core Under Constant Stress and Temperature; ASTM, USA.
- Bieniawski, Z.T. (1967), "Mechanism of brittle fracture of rock: Part II – Experimental studies", *Int. J. Rock Mech. Min. Sci.*, **4**(4), 407-423.
- Boukharov, G.N., Chanda, M.W. and Boukharov, N.G. (1995), "The three processes of brittle crystalline rock creep", *Int. J. Rock Mech. Min. Sci.*, **32**(4), 325-335.
- Chen, B.R., Zhao, X.J., Feng, X.T., Zhao, H.B. and Wang, S.Y. (2014), "Time-dependent damage constitutive model for the marble in the Jinping II hydropower station in China", *Bull. Eng. Geol. Environ.*, **73**(2), 499-515.
- Costin, L.S. (1985), "Time-dependent damage and creep of brittle rock", (In: *Damage Mechanics and Continuum Modeling*), *Proceedings of 2 Sessions Sponsored by the Engineering Mechanics Division of the American Society of Civil Engineering in Conjunction with the ASCE Convention*, Detroit, MI, USA, October.
- Cruden, D.M. (1971), "The form of the creep law for rock under uniaxial compression", *Int. J. Rock Mech. Min. Sci.*, **8**(2), 105-126.
- Cruden, D.M. (1974), "The static fatigue of brittle rock under uniaxial compression", *Int. J. Rock Mech. Min. Sci., Geomech. Abstr.*, **11**(2), 67-73.
- Cui, X.H. and Fu, Z.L. (2006), "Test study on rock creep properties and its long-term strength", *Chinese J. Rock Mech. Eng.*, **25**(5), 1021-1024.
- Donath, F.A. (1964), "Strength variation and deformational behavior in anisotropic rocks", *State of Stress in the Earth's Crust*, New York, NY, USA, pp. 281-300.
- Dusseault, M.B. and Fordham, C.J. (1993), "Time-dependent behavior of rocks", In: *Comprehensive Rock Engineering*, Oxford, Pergamon.
- Fabre, G. and Pellet, F. (2006), "Creep and time-dependent damage in argillaceous rocks", *Int. J. Rock Mech. Min. Sci.*, **43**(6), 950-960.
- Fujii, Y., Kiyama, T., Ishijima, Y. and Kodama, J. (1999), "Circumferential strain behavior during creep tests of brittle rocks", *Int. J. Rock Mech. Min. Sci.*, **36**(3), 323-327.
- He, M.C. and Xie, H.P. (2005), "Study on rock mechanics in deep mining engineering", *Chinese J. Rock Mech. Eng.*, **24**(16), 2803-2813.
- John, A.F. and Maurice, B.D. (1989), *Rock Engineering*, McGraw-Hill, New York, NY, USA.
- Hudson, J.A. (1971), "Effect of time on the mechanical behaviour of failed rock", *Nature*, **232**, 185-186.
- ISRM (1981), Rock characterization, testing and monitoring- ISRM Suggested method; Pergamon, Oxford, UK.
- Jin, J. and Cristescu, N.D. (1998), "An elastic-viscoplastic model for transient creep of rock salt", *Int. J. Plasticity*, **14**(1-3), 85-107.
- Korzeniowski, W. (1991), "Rheological model of hard rock pillar", *Rock Mech. Rock Eng.*, **24**(3), 155-166.
- Lajtai, E.Z. (1981), "Creep and crack growth in Lac du Bonnet granite due to compressive stress", *Proceedings of the 5th Canadian Fracture Conference on Fracture Problems and Solutions for the Energy Industry*, Winnipeg, MB, Canada, September, pp. 229-238.
- Lajtai, E.Z. (1991), "Time-dependent behaviour of the rock mass", *Geotech. Geolo. Eng.*, **9**(2), 109-124.
- Li, D.Y., Wong, L.N.Y., Liu, G. and Zhang, X.P. (2012), "Influence of water content and anisotropy on the strength and deformability of low porosity meta-sedimentary rocks under triaxial compression", *Eng. Geol.*, **126**, 46-66.
- Liu, M.Y. and Xu, C.Y. (2000), "Rheological properties of anhydrite and determination of its long time strength", *Chinese Min. Mag.*, **9**(2), 53-55.

- Liu, J., Yang, C.H., Wu, W. and Gao, X.P. (2006), "Study on creep characteristics and constitutive relation of rock salt", *Chinese Rock Soil Mech.*, **27**(8), 1267-1271.
- Luo, R.L. (2008), "Study on non-stationary creep model of deep lying rock and its application", Ph.D. Thesis; HoHai University, Nanjing, China.
- Ma, L. (2004), "Experimental investigation of time dependent behavior of welded Topopah Spring tuff", Dissertation; University of Nevada, Reno, NV, USA.
- Ma, L. and Daemen, J.J.K. (2006), "An experimental study on creep of welded tuff", *Int. J. Rock Mech. Min. Sci.*, **43**(2), 282-291.
- Malan, D.F. (1999), "Time-dependent behaviour of deep level tabular excavations", *Rock Mech. Rock Eng.*, **32**(2), 123-155.
- Malan, D.F. (2002), "Simulating the time-dependent behaviour of excavations in hard rock", *Rock Mech. Rock Eng.*, **35**(4), 225-254.
- Martin, C.D. and Chandler, N.A. (1994), "The progressive fracture of Lac du Bonnet granite", *Int. J. Rock Mech. Min. Sci.*, **31**(6), 643-659.
- Miura, K., Okui, Y. and Horii, H. (2003), "Micromechanics-based prediction of creep failure of hard rock for long-term safety of high-level radioactive waste disposal system", *Mech. Mater.*, **35**(3-6), 587-601.
- Munday, J.G.L., Mohamed, A.E. and Dhir, R.K. (1977), "A criterion for predicting the long-term strength of rock", *Proceedings of the Conference 'Rock Engineering' University of Newcastle-upon-Tyne*, Newcastle, England, April, pp. 127-135.
- Peng, S. (1973), "Time-dependent aspects of rock behavior as measured by a servo-controlled hydraulic testing machine", *Int. J. Rock Mech. Min. Sci. Geomech. Abstr.*, **10**(3), 235-246.
- Pushkarev, V.I. and Afanasev, B.G. (1973), "A rapid method of determining the long-term strengths of weak rocks", *J. Min. Sci.*, **9**(5), 558-560.
- Sangha, C.M. and Dhir, R.K. (1972), "Strength and complete stress-strain relationships for concrete tested in uniaxial compression under different test conditions", *Mate. Stru.*, **5**(6), 361-370.
- Shao, J.F., Zhu, Q.Z. and Su, K. (2003), "Modeling of creep in rock materials in terms of material degradation", *Comput. Geotech.*, **30**(7), 549-555.
- Shin, K., Okubo, S., Fukui, K. and Hashiba, K. (2005), "Variation in strength and creep life of six Japanese rocks", *Int. J. Rock Mech. Min. Sci.*, **42**(2), 251-260.
- Sterpi, D. and Gioda, G. (2009), "Visco-plastic behaviour around advancing tunnels in squeezing rock", *Rock Mech. Rock Eng.*, **42**(2), 319-339.
- Timoshenko, S.P. (1953), *History of Strength of Materials: With a Brief Account of the History of Theory of Elasticity and Theory of Structure*, McGraw-Hill, New York, NY, USA.
- Wang, G.J. (2004), "A new constitutive creep-damage model for salt rock and its characteristics", *Int. J. Rock Mech. Min. Sci.*, **41**(Supp. 1), 61-73.
- Wang, M.Y., Zhou, Z.P. and Qian, Q.H. (2006), "Tectonic, deformation and failure problems of deep rock mass", *Chinese J. Rock Mech. Eng.*, **25**(3), 448-455.
- Wang, J.B., Liu, X.R., Liu, X.J. and Huang, M. (2014), "Creep properties and damage model for salt rock under low-frequency cyclic loading", *Geomech. Eng., Int. J.*, **7**(5), 569-587.
- Wang, J.B., Liu, X.R., Song, Z.P. and Shao, Z.S. (2015), "An improved Maxwell creep model for salt rock". *Geomech. Eng., Int. J.*, **9**(4), 499-511.
- Wawersik, W.R. and Brace, W.F. (1971), "Post-failure behavior of a granite and diabase", *Rock Mech.*, **3**(2), 61-85.
- Xu, W.Y., Yang, S.Q. and Chu, W.J. (2006), "Nonlinear viscoelasto-plastic rheological model of rock and its engineering application", *Chinese J. Rock Mech. Eng.*, **25**(3), 433-447.
- Yang, S.Q. and Jiang, Y.Z. (2009), "Triaxial mechanical creep behavior of sandstone", *Min. Sci. Tech.*, **20**(3), 339-349.
- Yang, C.H., Daemen, J.J.K. and Yin, J.H. (1999), "Experimental investigation of creep behavior of salt rock", *Int. J. Rock Mech. Min. Sci.*, **36**(2), 233-242.
- Yang, W.D., Zhang, Q.Y., Li, S.C. and Wang, S.G. (2014), "Time-dependent behavior of diabase and a nonlinear creep model", *Rock Mech. Rock Eng.*, **47**(4), 1211-1224.

- Zhang, Q.Z., Shen, M.R. and Wen, Z. (2011), "Investigation on mechanical behavior of a rock plane using rheological tests", *J. Mater. Civ. Eng.*, **23**(8), 1220-1226.
- Zhang, Q.Z., Shen, M.R., Ding, W.Q. and Carl, C. (2012), "Shearing creep properties of cements with different irregularities on two surfaces", *J. Geophy. Eng.*, **9**(2), 210-217.
- Zhang, Y., Xu, W.Y., Gu, J.J. and Wang, W. (2013), "Triaxial creep tests of weak sandstone from fracture zone of high dam foundation", *J. Cent. South Univ.*, **20**(9), 2528-2536.
- Zhang, Y., Xu, W.Y., Shao, J.F., Zhao, H.B. and Wang, W. (2015), "Experimental investigation of creep behavior of clastic rock in Xiangjiaba Hydropower Project", *Water Sci. Eng.*, **8**(1), 55-62.
- Zhou, H. (2011), "A creep constitutive model for salt rock based on fractional derivatives", *Int. J. Rock Mech. Min. Sci.*, **48**(1), 116-121.
- Zhu, W., Li, Y., Li, S., Wang, S. and Zhang, Q. (2011), "Quasi-three-dimensional physical model tests on a cavern complex under high in-situ stresses", *Int. J. Rock Mech. Min. Sci.*, **48**(2), 199-209.

GC